Applied Physics Letters

Beamforming with transformation acoustics in anisotropic media

Cite as: Appl. Phys. Lett. **117**, 011907 (2020); https://doi.org/10.1063/5.0012974
Submitted: 07 May 2020 . Accepted: 30 June 2020 . Published Online: 09 July 2020

Steven R. Craig, Jeong Hun Lee, and Chengzhi Shi

Applied Physics Letters ARTICLE scitation.org/journal/apl

Beamforming with transformation acoustics in anisotropic media

Cite as: Appl. Phys. Lett. **117**, 011907 (2020); doi: 10.1063/5.0012974
Submitted: 7 May 2020 · Accepted: 30 June 2020 ·
Published Online: 9 July 2020

Steven R. Craig,[1] Jeong Hun Lee,[1] and Chengzhi Shi[1,2,a)]

AFFILIATIONS

[1]Meta Acoustic Lab, George W. Woodruff School of Mechanical Engineering, Georgia Institute of Technology, Atlanta, Georgia 30332, USA
[2]Parker H. Petit Institute for Bioengineering and Bioscience, Georgia Institute of Technology, Atlanta, Georgia 30332, USA

[a)]**Author to whom correspondence should be addressed:** chengzhi.shi@me.gatech.edu

ABSTRACT

Transformation acoustics correlates complex material properties in physical space with distorted wave manipulations in virtual space, such that wave propagation patterns can be determined by mathematical coordinate transformations. These transformations allow for accurate modeling of acoustic propagation in complex materials. Such models are relevant for both biomedical ultrasound therapies and integrated on-chip systems, where muscle fibers and piezoelectric substrates act as effective anisotropic media, respectively. Without considering the anisotropic density of these sophisticated media, attempts to beamform acoustic patterns by phase engineering result in a heavily distorted signal. This distortion is detrimental to the performance of high intensity focused ultrasound acoustic tweezers for noninvasive surgeries, cell trapping, and cell sorting. Here, we demonstrate that the distortion effects can be corrected by transformation acoustics in which the phased array profile is adjusted to account for the corresponding anisotropy. We perform experiments to verify this transformation acoustic correction for arbitrary focused and self-bending beams with two-dimensional anisotropic spoof surface acoustic waves. The benefit of transformation acoustics in suppressing undesired anisotropic effects on beamformed waves improves the precision and efficacy of medical treatments that facilitate noninvasive ultrasound therapies and integrated on-chip applications.

The constitutive relations that govern wave propagation through a medium directly depend on the physical properties of materials. This intrinsic relationship motivates researchers to create complex materials that manipulate wave propagation through mathematically defined coordinate transformations, known as transformation electromagnetics and acoustics.[1–3] This mapping leads to a unique design of wave bending and distortion that realizes electromagnetic and acoustic invisibility cloaks.[4–7] The transformation electromagnetics and acoustics are valid when the field equations describing wave propagation are invariant under coordinate transformations.[1,2] This is known to be true for Maxwell's field equations and enable the theoretical development of transformation electromagnetics.[8–10] Transformation invariance is also true for acoustics, given an anisotropic mass density tensor.[11,12] Transformation acoustics allows the design of acoustic metamaterials with effective anisotropic mass density properties that are used to experimentally demonstrate acoustic cloaking[5–7] and gradient index sonic lenses.[13–15]

On the other hand, transformation acoustics facilitates the mapping of wave patterns in sophisticated materials to medium where the precise modeling of wave propagation is well-understood. This is critical for high precision applications in which acoustic waves propagate through anisotropic media, with prime examples being biomedical acoustics and integrated on-chip systems. In recent years, biomedical ultrasound has demonstrated the ability to ablate cancerous tumors,[16–21] pulverize kidney stones,[22] and clear aortic plaque[23,24] in addition to being a noninvasive imaging tool for diagnostic purposes.[25–30] For many of these applications, beamforming by manipulating a phased array to generate a desired wave pattern in the body is critical [Fig. 1(a)]. In addition to applications for bulk acoustic waves, integrated on-chip systems use surface acoustic waves (SAWs) to manipulate, trap, and sort cells in a controlled environment.[31,32] These on-chip devices commonly use anisotropic piezoelectrics to support SAW propagation. For both bulk and surface acoustic waves, effective anisotropy distorts beamformed wave fronts and drastically affects the performance of the desired application [Fig. 1(b)]. To address these effects, we apply a coordinate transformation to correlate anisotropic wave distortion with a required phase profile correction. By doing so, any unwanted anisotropic effects are suppressed, and the intended beamforming is restored [Fig. 1(c)]. Here, we demonstrate the effectiveness of beamforming correction in anisotropic media

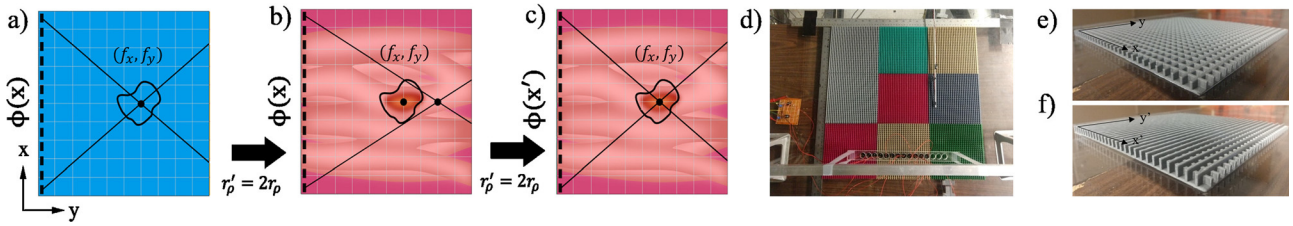

FIG. 1. (a) Discretized transducer array with a phase gradient as a function of the x axis such that the desired acoustic focusing is achieved in an isotropic medium. (b) Identical transducer array with the same phase gradient in an anisotropic medium, resulting in a focal point shifted from the desired location. (c) The same transducer array with a corrected phase gradient that restores the focal point to its original location. (d) Experimental setup in which two-dimensional SSAWs propagate across effective isotropic and anisotropic gratings. (e) Closeup of the isotropic grating design. (f) Closeup of the anisotropic grating design.

using transformation acoustics for biomedical and on-chip applications via experimental validation using finned grating surfaces that support two-dimensional spoof surface acoustic waves (SSAWs) for focused and self-bending beams [Fig. 1(d)].[33,34] Based on the dispersion relation of the grating,[35] we mimic effective isotropic [Fig. 1(e)] and anisotropic [Fig. 1(f)] media by varying the fin heights in x and y directions. First, we apply transformation acoustics to correct focused ultrasound beams in anisotropic media. The focusing of the acoustic waves in an isotropic medium can be achieved by a transducer array with the phase profile given by[36–40]

$$\phi(x) = -k_0\left[\sqrt{(x-f_x)^2 + (y-f_y)^2} - f_y\right], \tag{1}$$

where $\phi(x)$ is the transducer phase along the horizontal axis, k_0 is the wave number of the isotropic medium, and f_x and f_y are the coordinates of the focal point. The origin is set at the center of the transducer array. The focal point is chosen to be at (70 mm, 150 mm) for 9 kHz waves in our experiment. As expected, the phase gradient determined using Eq. (1) focuses the acoustic energy to the desired focal point in an isotropic medium in a numerical simulation [Fig. 2(a)]. On the other hand, the same phase profile of the transducer array results in a shifted focal spot in an anisotropic medium with the effective density 1.35 times greater in x than in y [Fig. 2(b)]. To correct for this shift, we map the coordinates (x, y) of the original isotropic medium to the coordinates (x', y') of the anisotropic medium with $x = [\sqrt{r_\rho}\cos(\theta)x' - \sin(\theta)y']$ and $y = [\sqrt{r_\rho}\sin(\theta)x' + \cos(\theta)y']$, where r_ρ is the ratio between the anisotropic density in the x' direction and the isotropic density, assuming that the anisotropic density in the y' direction is the same as the isotropic density and θ is the angle between the transducer array and the x' principle axis of the anisotropic medium. This coordinate transformation compensates the wavelength distortion along the principle axis due to the variance of sound speed as a result of the anisotropic density ($c_{x'} = c/\sqrt{r_\rho}$, where c and $c_{x'}$ are the sound speeds in the isotropic medium and along the x' axis in anisotropic medium, respectively). Substituting this transformation in Eq. (1) yields the corrected phase profile for focused acoustic beams in an anisotropic medium (see the supplementary material for details),

$$\phi(x', y') = -k_0\left[\sqrt{r_\rho(x'-f_x')^2 + (y'-f_y')^2} - \frac{\sqrt{r_\rho}\left(y'f_x' + x'f_y'\right)}{\sqrt{r_\rho x'^2 + y'^2}}\right]. \tag{2}$$

Applying this phase gradient with the aforementioned anisotropic density ratio shifts the focal point back to its intended location [Fig. 2(c)]. We perform experiments with the previously mentioned finned grating structures to verify the transformation. Isotropic and anisotropic grating surfaces were 3D printed and assembled from smaller square grating structures that combine to have a square surface area of $533 \times 533\,\text{mm}^2$ [Fig. 1(d)]. Small gaps or misalignments between gratings cause acoustic reflections that impact the beamforming performance, resulting in experimental error. The dispersion relation of the gratings determines the specific dimensions of each structure to mimic an effective isotropic or anisotropic medium (supplementary material). Acoustic surface waves were generated with a transducer array consisting of twelve 17 mm diameter speakers with a periodicity of 19 mm. The phase gradients were created using a digital multichannel recorder with independent channels to control the phase profile. To measure the resulted pressure field, an omnidirectional microphone attached to a motorized positioner scanned a planar area (5λ by 7λ, where the wavelength in the isotropic medium $\lambda = 38.1$ mm) 2 mm above the grating surfaces with a scan resolution of $\lambda/10$ for each case [Figs. 2(d)–2(f)]. A lock-in amplifier recorded the

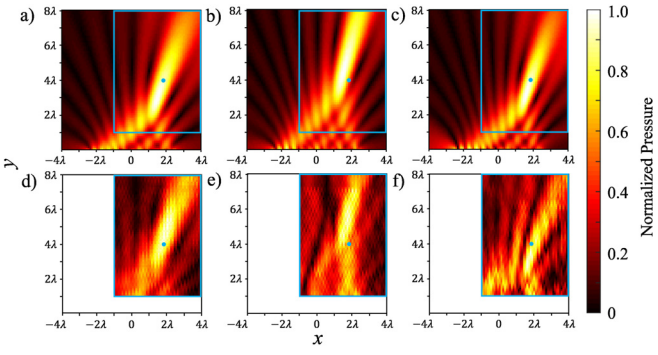

FIG. 2. (a) Simulation results of a focused acoustic beam in a 2D isotropic medium that focuses 70 mm to the right and 150 mm above the center of the speaker array. (b) Simulation results of a focused acoustic beam in an effective 2D anisotropic medium with the same phase profile as (a). Here, the resulting focal point shifts from the desired location. (c) Simulation results of a focused acoustic beam in an effective 2D anisotropic medium with a corrected phase profile with a focal point matching (a). (d) Experimental replication of the simulation in (a) with a matching focal point. (e) Experimental replication of the simulation in (b) with a matching focal point. (f) Experimental replication of the simulation in (c) with a matching focal point.

amplitude and phase of the acoustic waves to reconstruct the pressure fields above the grating surfaces. For an isotropic grating with a predetermined focal point at (70 mm, 150 mm) when the transducer array aligns with the x' axis, the acoustic intensity pattern matches with the desired focal point denoted by the blue dot in Fig. 2(d). When the same phase profile is applied to focus the acoustic wave on the anisotropic grating, the focal point shifts from the desired location to (57.15 mm, 209.55 mm) [Fig. 2(e)]. Using the corrected phase profile in Eq. (2), the focal point shifts back to its intended location [Fig. 2(f)].

The derived phase correction from transformation acoustics is also valid for more general cases in which the anisotropic axes are not in line with the speaker array. To demonstrate the focusing correction with misalignment, we tilt the transducer array 10° and focus the acoustic wave to the same focal spot at 9 kHz. The theoretical model focuses the acoustic energy at the predetermined location (the blue dot) as illustrated in Fig. 3(a). Again, switching the propagation medium to the anisotropic grating displaces the focal point to (38.1 mm, 215.65 mm) [Fig. 3(b)], while the corrected phase profile given by Eq. (2) restores the focal point to its proper location in Fig. 3(c). Experimental validation of the off-axis anisotropic density is performed using a nearly identical experimental setup as the previous case. However, the microphone's scan area is reduced to a 5λ by 6λ rectangular area [indicated by the blue rectangle in Figs. 3(a)–3(f)] to avoid collision with the tilted transducer array. The experimental demonstration with propagation above the isotropic grating results in a focal point [Fig. 3(d)] in agreement with the theoretical results shown in Fig. 3(a). Switching the grating surface to the anisotropic medium shifts the focal point [Fig. 3(e)], matching the results in Fig. 3(b), while applying the corrected phase profile shifts the focal point back to its intended location [Fig. 3(f)], matching Fig. 3(c).

To further demonstrate the effectiveness of transformation acoustics correcting anisotropic distortions, we restore the curved interference patterns of self-bending acoustic beams in anisotropic media. Without loss of generality, the resulting curved pattern of the

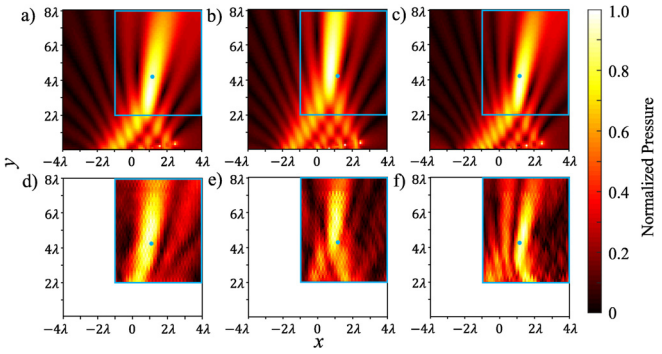

FIG. 3. (a) Simulation results of a focused acoustic beam in a 2D isotropic medium that achieves the desired focal point with a 10° tilt. (b) Simulation results of a focused acoustic beam with the same phase profile in an effective 2D anisotropic medium. Here, the focal point shifts from the focal point of the isotropic case. (c) Simulation results of a focused acoustic beam in an effective 2D anisotropic medium with a corrected phase profile resulting in focusing at the desired focal point (d) Experimental replication of (a) with a matching focal point. (e) Experimental replication of (b) with a matching focal point. (f) Experimental replication of (c) with a matching focal point.

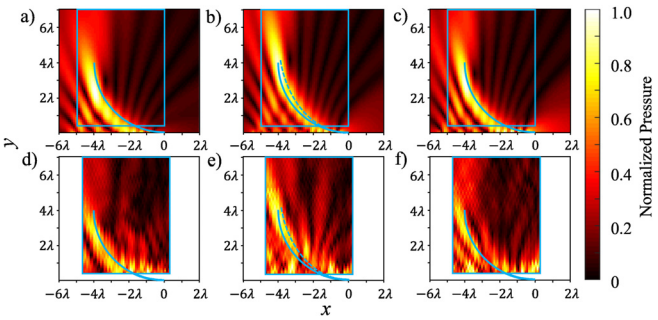

FIG. 4. (a) Simulation results of a self-bending acoustic beam in a 2D isotropic medium that matches the desired beam pattern. (b) Simulation results of a self-bending acoustic beam in an effective 2D anisotropic medium with the same phase profile. Here, the intensity profile shifts from the desired interference pattern. (c) Simulation results of a self-bending acoustic beam in an effective 2D anisotropic medium with a corrected phase profile. Here, the resulting curved interference pattern matches the desired intensity profile in the isotropic case. (d) Experimental replication of the simulation in (a) with a matching curved interference pattern. (e) Experimental replication of (b) with a matching interference pattern. (f) Experimental replication of (c) with a matching interference pattern.

acoustic beam is chosen to be $f(y) = \sqrt{r^2 - (y-r)^2}$, where r is the radius of the semicircular curve. The corresponding transducer array phase profile is derived in Refs. 36–40 and applied in an isotropic numerical simulation to achieve an acoustic energy intensity profile matching the aforementioned equation [Fig. 4(a)]. However, using the same phase profile on the transducer array in the previously discussed anisotropic medium distorts the semicircular interference pattern, resulting in an elliptical intensity profile [Fig. 4(b)]. We use transformation acoustics to restore the original semicircular pattern [Fig. 4(c)] by applying the same coordinate transformation as the focusing case to correct the phase gradient (supplementary material). To verify the transformation, we conduct experiments using the previously described experimental setup where the transducer array is in line with the x' axis. For an isotropic grating with a semicircular acoustic interference pattern having radius 4λ, the acoustic intensity pattern matches the desired trajectory denoted by the blue arc in Fig. 4(d). When the same phase profile is applied on the anisotropic grating, the circular trajectory distorts to form an elliptical arc [Fig. 4(e)]. Using the corrected phase profile (supplementary material), the beam is restored back to its intended interference pattern [Fig. 4(f)].

In conclusion, we use transformation acoustics to modify phase profiles for arbitrarily focused and self-bending acoustic beams to correct for the distortive effects resulted from anisotropy. Experimental verifications are performed using 2D grating structures that support SSAWs with density anisotropy in the x and y directions. This transformation acoustics enabled beamforming is crucial for biomedical ultrasound applications, such as high intensity focused ultrasound (HIFU), acoustic tweezers for noninvasive surgeries, cell trapping, and cell sorting.

See the supplementary material for the details of the corrected phase gradient derivations, the correction of high anisotropy cases, the grating dispersion, the effects of viscothermal loss, and additional full wave simulations.

This work was supported by Georgia Tech Faculty Startup Funding.

DATA AVAILABILITY

The data that support the findings of this study are available from the corresponding author upon reasonable request.

REFERENCES

[1]R. V. Craster and S. Guenneau, *Acoustic Metamaterials: Negative Refraction, Imaging, Lensing, and Cloaking* (Springer, Dordrecht, 2013), Chap. 8.
[2]H. Chen and C. T. Chan, "Acoustic cloaking and transformational acoustics," J. Phys. D **43**, 113001 (2010).
[3]F. Zhong, J. Li, H. Liu, and S. Zhu, "Controlling surface plasmons through covariant transformation of the spin-dependent geometric phase between curved metamaterials," Phys. Rev. Lett. **120**, 243901 (2018).
[4]J. Li and J. B. Pendry, "Hiding under the carpet: A new strategy for cloaking," Phys. Rev. Lett. **101**, 203901 (2008).
[5]B. Popa, L. Zigoneanu, and S. A. Cummer, "Experimental acoustics ground cloak in air," Phys. Rev. Lett. **106**, 253901 (2011).
[6]L. Y. Zheng, Y. Wu, X. Ni, Z. G. Chen, M. H. Lu, and Y. F. Chen, "Acoustic cloaking by a near-zero-index phononic crystal," Appl. Phys. Lett. **104**, 161904 (2014).
[7]M. Dubois, C. Shi, Y. Wang, and X. Zhang, "A thin and conformal metasurface for illusion acoustics of rapidly changing profiles," Appl. Phys. Lett. **110**, 151902 (2017).
[8]J. B. Pendry, D. Schurig, and D. R. Smith, "Controlling electromagnetic fields," Science **312**, 1780 (2006).
[9]U. Leonhardt, "Optical conformal mapping," Science **312**, 1777 (2006).
[10]D. Schurig, J. B. Pendry, and D. R. Smith, "Calculation of material properties and ray tracing in transformational media," Opt. Express **14**, 9794 (2006).
[11]S. A. Cummer and D. Schurig, "One path to acoustic cloaking," New J. Phys. **9**, 45 (2007).
[12]H. Chen and C. T. Chan, "Acoustic cloaking in three dimensions using acoustic metamaterials," Appl. Phys. Lett. **91**, 183518 (2007).
[13]A. Climente, D. Torrent, and J. Sanchez-Dehesa, "Sound focusing by gradient index sonic lenses," Appl. Phys. Lett. **97**, 104103 (2010).
[14]B. Popa and S. A. Cummer, "Design and characteristics of broadband acoustic composite metamaterials," Phys. Rev. B **80**, 174303 (2009).
[15]L. Zigoneanu, B. Popa, and S. A. Cummer, "Design and measurements of a broadband two-dimensional acoustic lens," Phys. Rev. B **84**, 024305 (2011).
[16]J. E. Kennedy, F. Wu, G. R. Ter Haar, F. V. Gleeson, R. R. Phillips, M. R. Middleton, and D. Cranston, "High-intensity focused ultrasound for the treatment of liver tumours," Ultrasonics **42**, 931–935 (2004).
[17]F. Wu, Z. B. Wang, W. Z. Chen, J. Z. Zou, J. Bai, H. Zhu, K. Q. Li, F. L. Xie, C. B. Jin, H. B. Su *et al.*, "Extracorporeal focused ultrasound surgery for treatment of human solid carcinomas: Early Chinese clinical experience," Ultrasound Med. Biol. **30**, 245–260 (2004).
[18]F. Wu, Z. B. Wang, W. Z. Chen, J. Bai, H. Zhu, and T. Y. Qiao, "Preliminary experience using high intensity focused ultrasound for the treatment of patients with advanced stage renal malignancy," J. Urol. **170**, 2237–2240 (2003).
[19]J. Ninet, X. Roques, R. Seitelberger, C. Deville, J. L. Pomar, J. Robin, O. Jegaden, F. Wellens, E. Wolner, C. Vedrinne *et al.*, "Surgical ablation of atrial fibrillation with off-pump, epicardial, high-intensity focused ultrasound: Results of a multicenter trial," J. Thorac. Cardiovasc. Surg. **130**, 803-e1 (2005).
[20]J. E. Kennedy, "High-intensity focused ultrasound in the treatment of solid tumours," Nat. Rev. Cancer **5**, 321 (2005).
[21]J. E. Kennedy, G. R. Ter Haar, and D. Cranston, "High intensity focused ultrasound: Surgery of the future?," Br. J. Radiol. **76**, 590–599 (2003).
[22]O. A. Sapozhnikov, A. D. Maxwell, B. MacConaghy, and M. R. Bailey, "A mechanistic analysis of stone fracture in lithotripsy," J. Acoust. Soc. Am. **121**, 1190–1202 (2007).
[23]Y. Takakuwa, M. Sarai, H. Kawai, A. Yamada, K. Shiino, K. Takada, Y. Nagahara, M. Miyagi, S. Motoyama, H. Toyama *et al.*, "Extracorporeal shock wave therapy for coronary artery disease: Relationship of symptom amelioration and ischemia improvement," Asia Ocean. J. Nucl. Med. Biol. **6**, 1 (2018).
[24]T. Nishida, H. Shimokawa, K. Oi, H. Tatewaki, T. Uwatoku, K. Abe, Y. Matsumoto, N. Kajihara, M. Eto, T. Matsuda *et al.*, "Extracorporeal cardiac shock wave therapy markedly ameliorates ischemia-induced myocardial dysfunction in pigs in vivo," Circulation **110**, 3055–3061 (2004).
[25]B. C. Tran, J. Seo, T. L. Hall, J. B. Fowlkes, and C. A. Cain, "Microbubble-enhanced cavitation for noninvasive ultrasound surgery," IEEE. Trans. Ultrason. Ferroelectr., Freq. Control **50**, 10 (2003).
[26]K. Hynynen, W. R. Freund, H. E. Cline, A. H. Chung, R. D. Watkins, J. P. Vetro, and F. A. Jolesz, "A clinical, noninvasive, MR imaging-monitored ultrasound surgery method," RadioGraphics **16**(1), 185 (1996).
[27]S. Wang, J. Lin, T. Wang, X. Chen, and P. Huang, "Recent advances in photoacoustic imaging for deep-tissue biomedical applications," Theranostics **6**, 2394 (2016).
[28]C. Errico, J. Pierre, S. Pezet, Y. Desailly, Z. Lenkei, O. Couture, and M. Tanter, "Ultrafast ultrasound localization microscopy for deep super-resolution vascular imaging," Nat. Lett. **527**, 499 (2015).
[29]M. Tanter and M. Fink, "Ultrafast imaging in biomedical ultrasound," IEEE Trans. Ultrason. Ferroelectr. Freq. Control **61**, 1 (2014).
[30]S. Jiménez-Gambín, N. Jiménez, J. M. Benlloch, and F. Camarena, "Holograms to focus arbitrary ultrasonic fields through the skull," Phys. Rev. Appl. **12**, 014016 (2019).
[31]D. J. Collins, A. Neild, and Y. Ai, "Highly focused high-frequency travelling surface acoustic waves (SAW) for rapid single-particle sorting," Lab Chip **16**, 471–479 (2016).
[32]A. Riaud, J. L. Thomas, M. Baudoin, and O. B. Matar, "Taming the degeneration of Bessel beams at an anisotropic-isotropic interface: Toward three-dimensional control of confined vortical waves," Phys. Rev. E **92**, 063201 (2015).
[33]T. Liu, F. Chen, S. Liang, H. Gao, and J. Zhu, "Subwavelength sound focusing and imaging via gradient metasurface-enabled spoof surface acoustic wave modulation," Phys. Rev. Appl. **11**, 034061 (2019).
[34]H. Jia, M. Lu, X. Ni, M. Bao, and X. Li, "Spatial separation of spoof surface acoustic waves on the graded groove grating," J. Appl. Phys. **116**, 124504 (2014).
[35]J. Zhu, Y. Chen, X. Zhu, F. J. Garcia-Vidal, X. Yin, W. Zhang, and X. Zhang, "Acoustic rainbow trapping," Sci. Rep. **3**, 1728 (2013).
[36]E. Greenfield, M. Segev, W. Walasik, and O. Raz, "Accelerating light beams along arbitrary convex trajectories," Phys. Rev. Lett. **106**, 213902 (2011).
[37]D. C. Chen, X. F. Zhu, Q. Wei, D. J. Wu, and X. J. Liu, "Dynamic generation and modulation of acoustic bottle-beams by metasurfaces," Sci. Rep. **8**, 12682 (2018).
[38]S. Zhao, Y. Hu, J. Lu, X. Qiu, J. Cheng, and I. Burnett, "Delivering sound energy along an arbitrary convex trajectory," Sci. Rep. **4**, 6628 (2015).
[39]J. Lan, X. Zhang, X. Liu, and Y. Li, "Wavefront manipulation based on transmissive acoustic metasurface with membrane-type hybrid structure," Sci. Rep. **8**, 14171 (2018).
[40]Y. Li, X. Jiang, R. Q. Li, B. Liang, X. Y. Zou, L. L. Yin, and J. C. Cheng, "Experimental realization of full control of reflected waves with subwavelength acoustic metasurfaces," Phys. Rev. Appl. **2**, 064002 (2014).